

Transcranial Electrical Stimulation and Recording of Brain Activity using Freestanding Plant-Based Conducting Polymer Hydrogel Composites

George D. Spyropoulos, Jeremy Savarin, Eliot F. Gomez, Daniel T. Simon, Magnus Berggren, Jennifer N. Gelinas, Eleni Stavrinidou,* and Dion Khodagholy*

Transcranial electrical stimulation is a noninvasive neurostimulation technique with a wide range of therapeutic applications. However, current electrode materials are typically not optimized for this abiotic/biotic interface which requires high charge capacity, operational stability, and conformability. Here, a plant-based composite electrode material based on the combination of aloe vera (AV) hydrogel and a conducting polymer (CP; poly(3,4-ethylenedioxythiophene):polystyrene sulfonate, PEDOT:PSS) is reported. This material system is fabricated into films and provides biocompatibility, conformability, and stability, while offering desirable electrical properties of the PEDOT:PSS. AVCP films are also molded onto the rough surface of the skull leading to a mechanically stable and robust interface. The *in vivo* efficacy of the AVCP films is verified to function as stimulating and recording electrodes by placing them on the skull of a rat and concomitantly inducing focal seizures and acquiring the evoked neural activity. AVCP films pave the way for high-quality biological interfaces that are broadly applicable and can facilitate advances in closed-loop responsive stimulation devices.

Transcranial electrical stimulation (TES) is an emerging neurostimulation technique with potential use for minimally invasive treatment of brain diseases.^[1] In contrast to deep brain

stimulation,^[2] TES employs two or more extracranial electrodes (placed on skull or scalp) to stimulate neural activity in the absence of direct contact with brain tissue. TES is categorized into three main types based on the stimulating waveform: direct current stimulation, alternating current stimulation, and random noise stimulation.^[3,4] During the stimulation phase, the potential difference between an electrode pair generates a current across skin, scalp, and skull that reaches the brain. A major emphasis in the TES field is investigating the mechanisms underlying its effects on brain tissue. Use of animal models is a key method to pursue this goal in an *in vivo* environment.^[1,5,6] In rodents, TES electrodes are placed on the surface of the skull to enable safe, chronic experimentation. Results derived from these models can be extrapolated to human subjects, where TES electrodes are placed on the

surface of the scalp, due to the relatively ohmic conducting properties of subcutaneous tissue.^[7–9]

The currently used TES electrodes are usually large (20–35 cm²) motivated by the need to reduce the electrochemical impedance of the electrode–tissue interface. This large surface area precludes their ability to provide local stimulation for high spatiotemporal resolution neuromodulation. Although smaller electrodes (1 cm²; similar to encephalography (electroencephalogram) electrodes) have been reported to establish more focal stimulation, multiple electrodes need to be combined to affect neural circuits.^[10] Commonly used TES electrode materials include metals, carbon-rubber, and self-adhesive hydrogels.^[11–13] Metal electrodes consist of a stainless steel or Ag/AgCl plate surrounded by a spongy or textile matrix that can uptake aqueous electrolyte and improve contact with tissue. However, evaporation of the electrolyte can increase the overall impedance and may create an unequal distribution of the electric field, potentially causing tissue damage and discomfort at the interface.^[4,14] Moreover, these electrodes are bulky and require elastic straps or supporting structures to maintain stable interfacing, thus hindering a reliable use of TES over an extended period of time.^[15] Carbon-rubber electrodes based on polysiloxane mixed with carbon powder can provide a flexible and soft electrode interface with tissue as compared to metal

Dr. G. D. Spyropoulos, J. Savarin, Prof. D. Khodagholy
Department of Electrical Engineering
Columbia University
New York, NY 10027, USA
E-mail: dk2955@columbia.edu

Dr. E. F. Gomez, Prof. D. T. Simon, Prof. M. Berggren, Prof. E. Stavrinidou
Laboratory of Organic Electronics
Department of Science and Technology
Linköping University
SE-601 74 Norrköping, Sweden
E-mail: Eleni.stavrinidou@liu.se

Prof. J. N. Gelinas
Department of Neurology
Columbia University Irving Medical Center
New York, NY 10032, USA

Prof. J. N. Gelinas
Institute for Genomic Medicine
Columbia University Irving Medical Center
630 W 168th St., New York, NY 10032, USA

 The ORCID identification number(s) for the author(s) of this article can be found under <https://doi.org/10.1002/admt.201900652>.

DOI: 10.1002/admt.201900652

electrodes. However, they still require aqueous electrolyte and sponge structures at the interface to provide efficient charge delivery to target tissue.^[4] To extend the operation time of wet sponge-based electrodes, poly acrylics and *N*-vinylpyrrolidone-based hydrogels have been fabricated on a conductive substrate to establish a flexible and adhesive electrode.^[12] However, these electrode setups require a large surface area due to their high electrochemical impedance. In addition, it is challenging to miniaturize and manufacture these devices because of their multistack architecture of the functional layers (adhesive, electrical, and ionic conducting layers). Such an arrangement increases the thickness of the device and prevents creation of a slim and conformable interface with tissue. Ideal TES electrodes should be i) conformable, flexible, and nonbulky, ii) biocompatible and stable in physiological environments, iii) high charge capacity for effective interaction with electrophysiological signals, and iv) mechanically self-supporting to skull or tissue.

We hypothesized that by combining high charge capacity mixed-conducting polymers and biocompatible hydrophilic gels, it would be possible to create TES electrode that fulfill these criteria. Poly(3,4-ethylenedioxythiophene):polystyrene sulfonate (PEDOT:PSS) and other conducting polymers such as polypyrrole and polyaniline have been widely used to formulate hydrogel-based bioelectronics for neural interface applications.^[16–22] These hydrogels are comprised of a cross-linking system enriched with a hydrating medium that can be biological or synthetic (such as polysaccharides or polymethacrylates, respectively).^[18] Hydrogel films can also be created using PEDOT:PSS without addition of a hydrating medium.^[19] PEDOT:PSS can be combined with nanofibrillated cellulose to generate a freestanding film with paper-like properties.^[23] Such a film demonstrates high charge capacity and improved combined electronic-ionic conduction compared to thick PEDOT:PSS films alone because the conducting polymer wraps around individual nanocellulose fibers and increases the effective surface area.^[24] However, extraction of high-quality nanocellulose fibers from pulp requires extensive processing with sophisticated equipment. Therefore, we aimed to leverage the high conductivity of PEDOT:PSS in combination with a biologically derived hydrating medium with a facile extraction process. Aloe vera (AV) gel is a widely used plant-based hydrogel naturally enriched with amino acids, lipids, sterols, vitamins, and saccharides that could fulfill this function.^[25,26] It has been used in a wide variety of applications, ranging from cosmetics and the food industry to wound healing, tissue engineering, and drug delivery systems.^[25–27] AV gel has, nevertheless, rarely been harnessed for use in bioelectronics.^[28]

Here, we report a fully solution-processed, biocompatible, high charge capacity, mixed conducting polymer hydrogel material that can be used to create conformable, freestanding TES electrodes capable of self-supported contact with skull in a rodent model. AV gel was extracted directly from the plant and it was combined, without any sophisticated processing, with the conducting polymer PEDOT:PSS, additive plasticizers, and surfactants in a composite film (AVCP) to form TES material. The self-supporting mechanical properties of the gel were complemented by the ionic and electronic conductivity of the conducting polymer. Electrochemical characterization revealed that the film provides a high charge capacity and establishes a low

electrochemical impedance interface with the skull. To validate its efficacy for TES, we used the AVCP film to fabricate TES electrodes and found that they exhibited lower *in vivo* electrochemical impedance and higher charge capacity compared to conventional metal-based TES electrodes. AVCP-based TES electrodes were able to modulate activity of neurons in the rat brain *in vivo*, delivered sufficient charge to induce epileptic activity, and concomitantly recorded neural activity from multiple brain regions.

To create an AV-based film with mixed ionic and electronic conduction, we optimized a mixture of AV gel extracted from the aloe vera succulent plant and the conducting polymer PEDOT:PSS (AVCP films; Figure S1, Supporting Information). AV gel supported the formation of a stable biocompatible matrix that was fully blended with the PEDOT:PSS. By varying the weight ratio between the AV and PEDOT:PSS, we were able to achieve an optimal balance between low electrochemical impedance, stability for mechanical manipulation, and adequate hydration. A weight ratio percentage of 42.5% AV to 53.6% PEDOT:PSS achieved the lowest electrochemical impedance values across the majority of the physiological frequency spectrum. In the high frequency regime ($>3 \times 10^5$ Hz), a combination of 62.5% AV to 33.6% PEDOT:PSS exhibited lower values. Regardless of composition percentage, AVCP films displayed significantly improved impedance compared to a Au electrode of equal dimensions (Figure 1A,B). To gain more insight into the charge capacity of the optimized AVCP films compared to crosslinked PEDOT:PSS and bare Au interfaces, we performed cyclic voltammetry (CV). AVCP films had wide box-shaped CV profiles, indicating that capacitive processes dominate the charge interaction at the interface. In contrast, the Au electrode exhibited a resistive profile (Figure 1C and Figure S2, Supporting Information). These results support the hypothesis that AVCP films have high volumetric capacitance, in contrast to the formation of an electrical double layer capacitance on the Au interface.^[29–31] AVCP films displayed a CV profile with a larger area than PEDOT:PSS films of similar dimensions and polymer content, demonstrating that AV increased the charge capacity of the CP films (1.3 mF instead of 1 mF for pure PEDOT:PSS film), likely due to higher porosity (Figure S3, Supporting Information).^[32] This result was further supported by the larger micron-scale pores in PEDOT:PSS films compared to AVCP films as quantified by comparative transmission polarized optical microscopy (Figure S3, Supporting Information).

Key properties for a reliable TES electrode material are mechanical and chemical stability in a biological environment. To evaluate these properties, we compared AVCP films with a series of PEDOT:PSS-based composites fabricated into freestanding films with comparable ionic conductivity and biocompatibility (Figure 1D). PEDOT:PSS-based composite films made with chitosan (CS) and CS/polyvinyl alcohol (PVA) were mechanically self-supporting and were able to generate freestanding films in dry conditions. However, only the AVCP and PEDOT:PSS films cross-linked with (3-glycidyloxypropyl)trimethoxysilane (GOPS) showed mechanical resilience in hydrated conditions. To test the mechanical stability and robustness of AVCP film, we have performed tensile strength measurements (Figure S4, Supporting Information). Stress versus strain characteristics resulted in a Young's modulus of 0.154 GPa.^[33] AVCP film with thickness of 50 μm , and

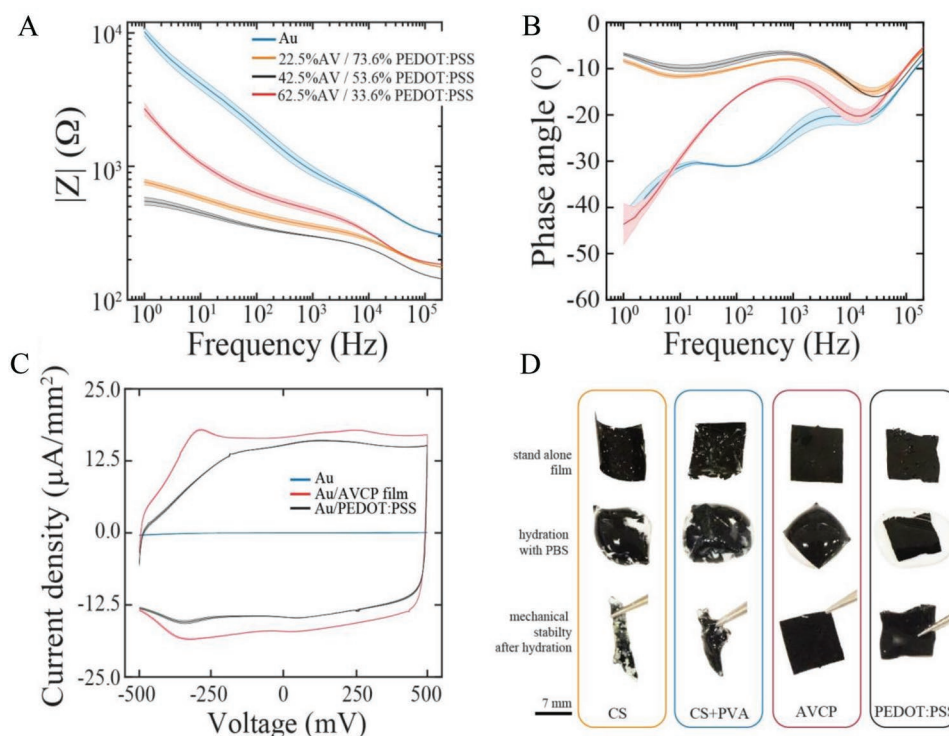


Figure 1. Addition of AV gel to PEDOT:PSS creates a stable conducting polymer film. A) EIS of Au (blue), Au/22.5% AV/73.6% PEDOT:PSS (orange), Au/42.5% AV/53.6% PEDOT:PSS (black), and Au/62.5% AV/33.6% PEDOT:PSS (red) 4 mm² electrodes. Mean values (solid line) and standard deviation (shaded area) are shown for $n = 5$. B) Phase plots for the corresponding electrochemical impedance measurements. Mean values (solid line) and standard deviation (shaded area) are shown for $n = 5$. C) Cyclic voltammograms of Au (blue), Au/AVCP (red), and Au/PEDOT:PSS (black) 4 mm² electrodes in PBS at 50 mV s⁻¹. Mean values (solid line) and standard deviation (shaded area) are shown for $n = 5$. Area calculation of the mean values resulted in a corresponding capacitance of 5.5 μ F (Au), 1.3 mF (Au/AVCP), and 1 mF (Au/PEDOT:PSS). D) Mechanical stability of various freestanding conducting polymer films before and after hydration. Raw images of chitosan (orange), chitosan/PVA (blue), AV-based (red), and pure PEDOT:PSS (black) films were compared after fabrication (top) and after hydration in PBS (middle and bottom). The AVCP film shows mechanical integrity after hydration with PBS.

a cross-sectional area of 1 mm², could withstand up to 14 N of tensile force. Overall, AVCP films were found to have high charge capacity as well as the ability to maintain mechanical stability in aqueous environments and under tensile strength.

We next sought to characterize the electrical properties and charge carrier mobility of the AVCP film. To accomplish this characterization, we fabricated organic electrochemical transistors (OECTs) with a channel composed of AVCP. AVCP operated as a depletion mode transistor channel material, such that when a positive voltage between the AVCP source and the Ag/AgCl gate was applied, ions diffused from the electrolyte in the channel to compensate the sulfonate anions of the PSS, reducing the hole density in the PEDOT and reversibly decreasing the channel current (Figure 2A).^[34] These AVCP-based transistors delivered high current (≈ 90 mA for drain voltage (V_D) of -0.6 V and gate voltage (V_G) of 0 V) with a maximum transconductance of 250 mS (Figure 2B and Figure S5, Supporting Information). This high transconductance value is likely attributed to the highly homogenous distribution of PEDOT:PSS throughout the entire thickness of AV matrix (≈ 40 μ m) that results in a large volumetric capacitance, consistent with results obtained with impedance spectroscopy and CV measurements.^[35] Assuming that AVCP-based OECTs operate in the saturation regime $|V_D| > |V_G|$, we can estimate

the mobility of the channel material from the square root of the transfer characteristics of the device (Figure 2C).^[36,37] We found high mobility values ($\mu_{\text{sat}} = 2.59$ cm² V⁻¹ s⁻¹) that were similar to the mobility of films consisting of only PEDOT:PSS,^[38] suggesting that addition of AV does not compromise the electronic properties of PEDOT:PSS.

Mechanically reliable contact with biological tissue is necessary for consistent delivery of charge through TES electrodes.^[12] We found that AVCP films can stably conform to the surface of the skull without addition of any other chemicals (Figure 3A). In the presence of excess water at the AVCP–skull interface, we found that the gel-based film took up water and became softer, allowing it to follow the rough and porous surface of the skull. After removal of the excess water, the film maintained its topography. Scanning electron microscopy (SEM) images of the AVCP–skull interface confirmed that AVCP film “molds” to the skull, creating an optimal mechanical contact. This behavior is likely attributable to the saccharide-rich composition of the AV gel.^[39] Subsequently, we investigated the properties of AVCP films in vivo. Under isoflurane anesthesia, we placed an AVCP film and Au electrodes on the surface of a rat skull and performed impedance spectroscopy. The AVCP film demonstrated reduced electrochemical impedance over a broad frequency range (0.1–10⁶ Hz) compared to the Au electrodes in the

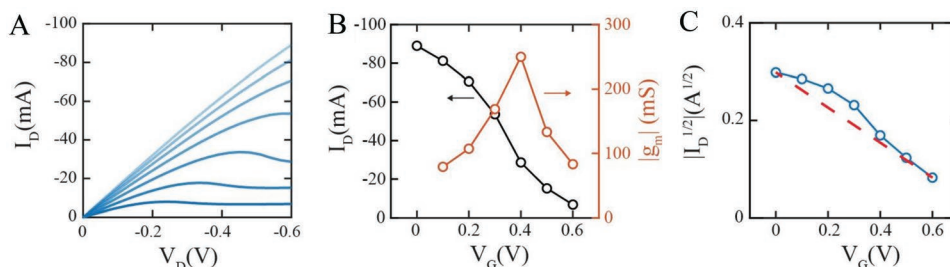


Figure 2. Steady-state characteristics of AVCP film-based OECTs. A) Output characteristics ($I_D - V_D$) of AVCP film-based OECT device ($L = 250 \mu\text{m}$, $W = 1000 \mu\text{m}$) for gate voltage (V_G) varying from 0 V (top curve) to +0.6 V (bottom curve) with a step of +0.1 V; color intensity corresponds to V_G amplitude (I_D , V_G , and V_D denote drain current, gate voltage, and drain voltage). B) Transfer curve for $V_D = -0.6 \text{ V}$ (black), and the corresponding transconductance (orange), $|g_m|_{\text{max}} = 250 \text{ mS}$. C) Square root transfer curve characteristics; mobility in the saturation regime can be found by linear fitting as described by the equations in, $\mu_{\text{sat}} = 2.59 \text{ cm}^2 \text{ V}^{-1} \text{ s}^{-1}$.

absence of any additional hydration (Figure 3C and Figure S6, Supporting Information). Measurements were made using two #000-gauge surgical stainless steel screws implanted over the

cerebellum of the rat to serve as reference and counter electrodes. Both interfaces had higher overall impedance compared to in vitro measurements, likely resulting from the increased

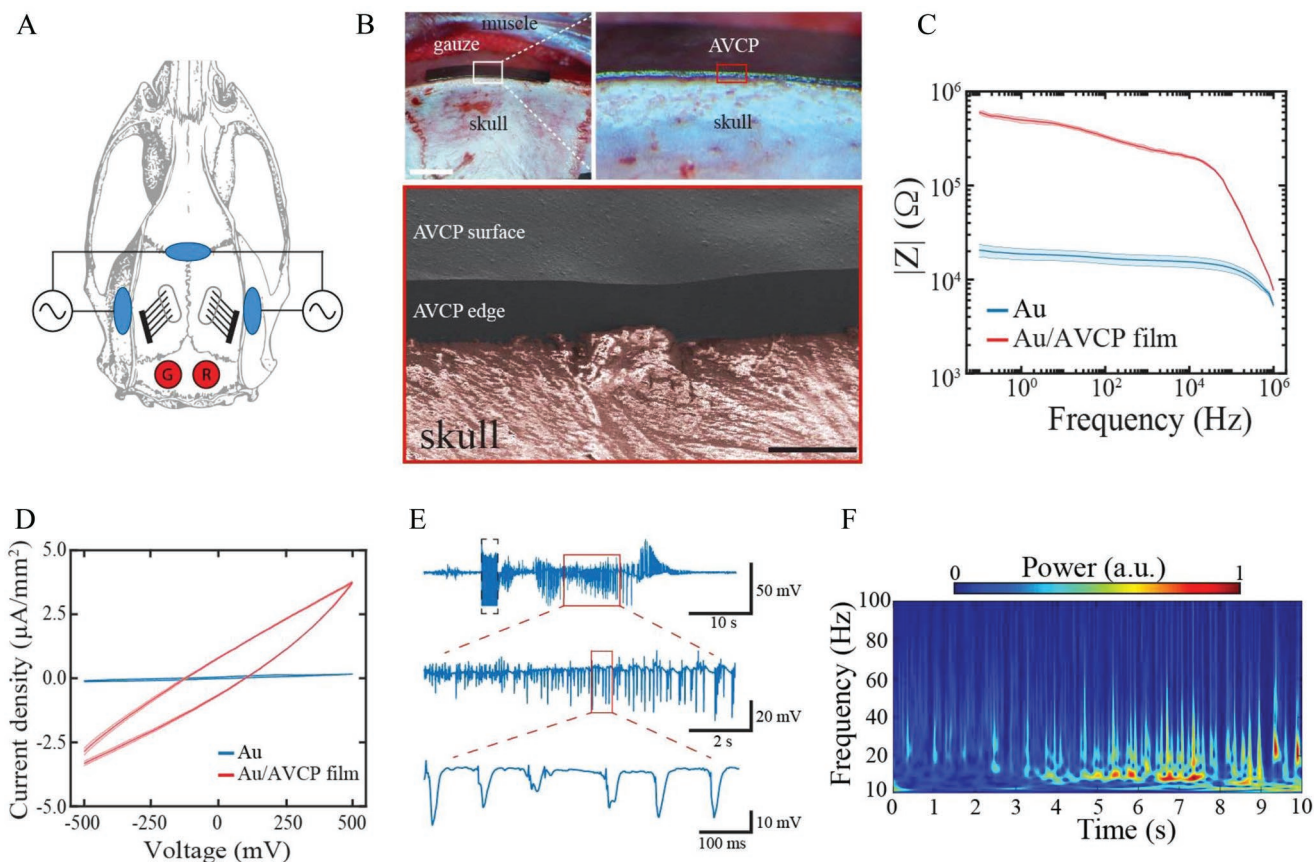


Figure 3. AVCP-based TES electrodes enable focal seizure stimulation in vivo. A) Illustration of TES electrodes (blue) and reference/ground electrode (red) position on the skull surface. Two cranial windows with implantable microwires are illustrated. B) Optical micrograph displaying the top view of the left parietal bone and an AVCP film conforming to the rat skull. Scale bar 2 mm. Inset shows a zoomed-in optical image of the same area. Red box displays a cross-sectional SEM image showing the interface between an AVCP film (black) and a rat skull (copper). Scale bar $50 \mu\text{m}$. C) In vivo EIS of Au (blue) and Au/AVCP film (red) 4 mm^2 electrodes. Mean values (solid line) and standard deviation (shaded area) are shown for $n = 5$. D) In vivo cyclic voltammogram of Au (blue) and Au/AVCP film (red) 4 mm^2 electrodes at 50 mV s^{-1} . Mean values (solid line) and standard deviation (shaded area) are shown for $n = 5$. E) Epileptic seizure induced and recorded by AVCP-based TES electrodes placed intra-operatively on the rat skull. Upper time trace shows 50 s of pre-ictal activity, stimulation artifact (black dotted box), induced epileptic seizure, and post-ictal activity as recorded by AVCP-based TES electrodes placed on the vertical ridges of a rat skull. Insets (red boxes) demonstrate higher temporal resolution of the evoked epileptic discharges. F) Time-frequency spectrogram of the evoked seizure acquired through AVCP-based TES electrodes. Warmer colors represent higher relative power.

resistance of the path between working and reference electrodes (phosphate-buffered saline (PBS) vs skull, dura, and intracranial tissue). Increasing the surface areas of the reference electrode did not result in significant changes in the CV curves, confirming that the more resistive *in vivo* CV profile arose from the biological environment rather than the reference electrode arrangement.^[8,40] No distinct peaks were observed during *in vivo* CV measurements, suggesting that AVCP films are governed by purely capacitive processes and do not engage in any redox reactions in a physiological environment (Figure 3D).^[31]

We then used the AVCP film as both recording and TES electrodes to acquire high-quality brain signals and stimulate neural activity. Three $2 \times 3 \text{ mm}^2$ strips of AVCP films were maintained on the surface of the rat skull without the need of any additional adhesives or hydration. Two AVCP-based electrodes were placed on the left and right lateral surfaces of skull, over the temporal region to serve as working electrodes.^[1] One AVCP-based electrode was placed on the dorsal frontal midline of the skull to serve as the stimulation reference electrode. In addition, two arrays of 50 μm tungsten wire electrodes were implanted bilaterally into both hippocampi (anterior–posterior = 3.5 mm, medial–lateral = 3.0 mm, dorsal–ventral = 2.0 mm). Two screws over the cerebellum again served as ground and reference electrodes for neural recordings. With this configuration, we recorded neurophysiological signals characteristic of brain activity under isoflurane anesthesia with the AVCP electrodes (Figure 3E and Figure S2, Supporting Information). The high signal-to-noise ratio data obtained with AVCP electrodes was consistent with stable electronic and mechanical interface with the skull. Next, we used the AVCP electrodes to apply current, directly investigating their functionality as TES electrodes. We applied current through the AVCP electrodes with parameters previously shown to induce epileptic seizures when applied intracranially (10 ms duration biphasic pulses for a period of 2 s;^[41,42] Figure S7 in the Supporting Information, black dashed line box shows stimulation artifact). Current application at 3 mA induced an epileptic seizure, characterized by high amplitude, broad band, evolving spike, and wave discharges lasting for approximately 30 s (Figure 3E,F). We demonstrated that the AVCP-based TES electrodes induced a spatially localized response because electrodes implanted in distinct regions displayed different electrophysiological patterns (Figure S6, Supporting Information). Therefore, AVCP-based TES electrodes on the skull can generate sufficient intracranial charge in targeted brain regions to drive neurons to epileptic activity.

In summary, we demonstrated a high charge capacity, free-standing, plant-based composite material that can be used to transcranially stimulate and record brain activity. These electrodes were fabricated via a simple and inexpensive process. The combination of PEDOT:PSS and AV gel provided biocompatibility, conformability, and stability, and did not alter the desirable electrical properties of PEDOT:PSS. The AV gel-based film molded onto the rough surface of the skull, leading to a mechanically stable interface. We verified the *in vivo* efficacy of the AVCP electrodes by placing them on the skull of a rat and concomitantly inducing focal seizures and recording the evoked neural activity. We also compared the *in vivo* electrochemical impedance and CV of AVCP-based TES electrodes with conventional Au-based TES electrodes. AVCP results in several orders

of magnitude lower impedance and higher charge capacity relative to metal electrodes, indicating that hydrogels can be leveraged to increase the efficiency of charge transfer^[22,43] for TES. AVCP films pave the way for high-quality biological interfaces that can advance closed loop responsive stimulation devices in wearable electronics and therapeutic devices.

Experimental Section

Fabrication of AVCP Film: PEDOT:PSS (Clevios PH1000) was acquired from Heraeus. Dimethyl sulfoxide (DMSO) and glycerol were purchased from Sigma-Aldrich. AV gel was extracted directly from the leaves of an aloe vera plant just before use. The gel was passed through a metallic mesh (1 mm²) and then homogenized with a T10 Basic ULTRA TURRAX homogenizer for 10 min at speed setting 3 and 1 min at speed setting 4. The beaker with the gel was placed in a cold bath to avoid heating during homogenization. PEDOT:PSS, DMSO, and glycerol were added and then the mixture was homogenized again for 6 min (5 min-setting 3 and 1 min-setting 4). The mixture was then placed in desiccator overnight to degas. Then it was poured into a petri dish and dried in an oven at 60 °C. Various concentrations of PEDOT:PSS, AV gel, DMSO, and glycerol were tested and the optimal concentration of 42.5/53.6/3.3/0.6 wt% was found. The final film was patterned by a sharp blade to give the desired electrode shape.

Fabrication of OECT: Ti (10 nm) and Au (100 nm) layers were deposited with an e-beam metal evaporator on cleaned glass substrates (1 mm thickness). A thin PEDOT:PSS layer ($\approx 20 \text{ nm}$) was spin coated, dried, and patterned on top of gold contacts by peel-off process. A second thin PEDOT:PSS layer ($\approx 20 \text{ nm}$) was spin coated and patterned in a similar process. Before the layer dried, an AVCP film was laminated on top to realize the channel. Robust contacts between Au/PEDOT:PSS and AVCP were achieved with subsequent thermal treatment at 120 °C and drying of the second PEDOT:PSS layer.

Mechanical Stability: To evaluate the mechanical stability of the optimized AVCP films, these were compared with various PEDOT:PSS-based films (PEDOT:PSS/CS (10 wt%), PEDOT:PSS/CS/PVA (10 wt%), and standalone PEDOT:PSS/GOPS (1 wt%) films) in dry and hydrated conditions. Hydration was provided with standard PBS solution.

Electrical Characterization: Current–voltage characteristics were measured with a Keysight B2902A Precision Source/Measurement Unit using two channels. On the first channel (V_D), linear sweeps from 0 to -0.6 V with a step of -0.03 V were applied. On the second channel (V_G), constant voltages from 0 to 0.6 V with a step of 0.1 V were applied. The electrical characteristics of the AVCP-based OECT were measured with $1 \times \text{PBS}$ as an electrolyte and Ag/AgCl as gate electrode. Electrochemical impedance spectroscopy (EIS) and CV were performed with a Gamry Instruments Reference 600+ using a three-electrode configuration with platinum and Ag/AgCl as counter and reference electrodes, respectively. Au, PEDOT:PSS, or AVCP working electrodes with identical geometry (4 mm²) were used.

SEM images were acquired with a Zeiss Sigma VP scanning electron microscope. Before imaging the devices, an $\approx 10 \text{ nm}$ AuPd layer was sputtered. The SEM images were taken with an acceleration voltage of 5 kV. AVCP or PEDOT:PSS freestanding films were laminated onto Au contacts as described previously for fabrication of OECTs.

TES and Recording: Animal protocols were approved by the Institutional Animal Care and Use Committee of Columbia University. Three male and female Long Evans rats (200–350 g, 8–15 wks of age) were used for TES and recording. Rats were kept on a regular 12–12 h light dark cycle, housed in pairs prior to surgical procedure, and euthanized immediately afterward. The animals were initially anaesthetized with 2% isoflurane and maintained under anesthesia with 0.75–1% isoflurane during the surgery. The head of the rat was immobilized in a stereotaxic apparatus and the body temperature was kept at 37.5 °C. A longitudinal incision was made in the scalp and the dorsal and lateral aspects of the skull were exposed. A stainless-steel screw was driven into the skull above the cerebellum to serve as ground and reference electrodes. Seizure stimulation was consisted of

2 s duration bipolar current pulses (60 Hz, 10 ms pulse width). Current was titrated until observable seizure activity occurred. Neural activity was recorded using AVCP-based electrodes, amplified, and digitized continuously at 20 kHz using a head-stage directly attached to the electrodes (RHD2000 Intan technology), and stored for off-line analysis with 16-bit format. Data were analyzed using MATLAB (MathWorks) and visualized using Neuroscope. Spectrograms were generated using wavelet transformation (Gabor).

Supporting Information

Supporting Information is available from the Wiley Online Library or from the author.

Acknowledgements

This work was supported by Columbia University School of Engineering and Applied Science and Columbia University Irving Medical Center Department of Neurology and Institute for Genomic Medicine. G.D.S. is supported through the Human Frontiers Postdoctoral Fellowship Program (LT000831/2017-C). The authors thank all Khodagholy and Gelinas laboratory members for their support. E.S. was supported by a Marie Skłodowska Curie Individual Fellowship (MSCA-IFEF-ST, Trans-Plant, 702641) and a VR starting grant. Additional funding was provided by Vetenskapsrådet (VR-, VR-) Knut and Alice Wallenberg Foundation and the Swedish Government Strategic Research Area in Materials Science on Functional Materials at Linköping University (Faculty Grant SFO-Mat-LiU No. 2009-00971).

Conflict of Interest

The authors declare no conflict of interest.

Keywords

aloe vera, hydrogel, PEDOT:PSS, transcranial electrical stimulation (TES)

Received: July 30, 2019

Revised: October 8, 2019

Published online:

- [1] M. Vöröslakos, Y. Takeuchi, K. Brinyiczki, T. Zombori, A. Oliva, A. Fernández-Ruiz, G. Kozák, Z. T. Kincses, B. Iványi, G. Buzsáki, A. Berényi, *Nat. Commun.* **2018**, *9*, 483.
- [2] D. Benninger, M. Schüpbach, *Ther. Umsch.* **2018**, *75*, 425.
- [3] T. Reed, R. Cohen Kadosh, *J. Inherited Metab. Dis.* **2018**, *41*, 1123.
- [4] R. C. Kadosh, *The Stimulated Brain: Cognitive Enhancement using Non-Invasive Brain Stimulation*, Elsevier, New York **2014**.
- [5] S. Ozen, A. Sirota, M. A. Belluscio, C. A. Anastassiou, E. Stark, C. Koch, G. Buzsáki, *J. Neurosci.* **2010**, *30*, 11476.
- [6] A. Berényi, M. Belluscio, D. Mao, G. Buzsáki, *Science* **2012**, *337*, 735.
- [7] N. Grossman, D. Bono, N. Dedic, S. B. Kodandaramaiah, A. Rudenko, H. J. Suk, A. M. Cassara, E. Neufeld, N. Kuster, L. H. Tsai, A. Pascual-Leone, E. S. Boyden, *Cell* **2017**, *169*, 1029.
- [8] S. F. Lempka, S. Miocinovic, M. D. Johnson, J. L. Vitek, C. C. McIntyre, *J. Neural Eng.* **2009**, *6*, 046001.
- [9] D. Liebetanz, R. Koch, S. Mayenfels, F. König, W. Paulus, M. A. Nitsche, *Clin. Neurophysiol.* **2009**, *120*, 1161.
- [10] J. P. Dmochowski, A. Datta, M. Bikson, Y. Su, L. C. Parra, *J. Neural Eng.* **2011**, *8*, 046011.
- [11] C. G. Sinks, M. Nonte, W. D. Hairston, in *2019 9th Int. IEEE/EMBS Conf. Neural Engineering (NER)*, IEEE, Piscataway, NJ **2019**, pp. 678–681.
- [12] T. Keller, A. Kuhn, *J. Autom. Control* **2008**, *18*, 35.
- [13] D. Wirthl, R. Pichler, M. Drack, G. Kettlgluber, R. Moser, R. Gerstmayr, F. Hartmann, E. Bradt, R. Kaltseis, C. M. Siket, S. E. Schausberger, S. Hild, S. Bauer, M. Kaltenbrunner, *Sci. Adv.* **2017**, *3*, e1700053.
- [14] A. S. Oliveira, B. R. Schlink, W. D. Hairston, P. König, D. P. Ferris, *J. Neural Eng.* **2016**, *13*, 036014.
- [15] A. F. DaSilva, M. S. Volz, M. Bikson, F. Fregni, *J. Vis. Exp.* **2011**, e2744.
- [16] R. Green, *Nat. Biomed. Eng.* **2019**, *3*, 9.
- [17] Y. Liu, J. Liu, S. Chen, T. Lei, Y. Kim, S. Niu, H. Wang, X. Wang, A. M. Foudeh, J. B.-H. Tok, Z. Bao, *Nat. Biomed. Eng.* **2019**, *3*, 58.
- [18] J. Goding, C. Vallejo-Giraldo, O. Syed, R. Green, *J. Mater. Chem. B* **2019**, *7*, 1625.
- [19] B. Lu, H. Yuk, S. Lin, N. Jian, K. Qu, J. Xu, X. Zhao, *Nat. Commun.* **2019**, *10*, 1043.
- [20] R. Green, M. R. Abidian, *Adv. Mater.* **2015**, *27*, 7620.
- [21] U. A. Aregueta-Robles, A. J. Woolley, L. A. Poole-Warren, N. H. Lovell, R. A. Green, *Front. Neuroeng.* **2014**, *7*, 15.
- [22] R. A. Green, S. Baek, L. A. Poole-Warren, P. J. Martens, *Sci. Technol. Adv. Mater.* **2010**, *11*, 014107.
- [23] F. Jiao, J. Edberg, D. Zhao, S. Puzinas, Z. U. Khan, P. Mäkie, A. Naderi, T. Lindström, M. Odén, I. Engquist, M. Berggren, X. Crispin, *Adv. Sustainable Syst.* **2018**, *2*, 1700121.
- [24] A. Malti, J. Edberg, H. Granberg, Z. U. Khan, J. W. Andreasen, X. Liu, D. Zhao, H. Zhang, Y. Yao, J. W. Brill, I. Engquist, M. Fahlman, L. Wågberg, X. Crispin, M. Berggren, *Adv. Sci.* **2016**, *3*, 1500305.
- [25] A. Balaji, M. V. Vellayappan, A. A. John, A. P. Subramanian, S. K. Jaganathan, M. SelvaKumar, A. A. bin Mohd Faudzi, E. Supriyanto, M. Yusuf, *RSC Adv.* **2015**, *5*, 86199.
- [26] A. Surjushe, R. Vasani, D. G. Saple, *Indian J. Dermatol.* **2008**, *53*, 163.
- [27] M. Irimia-Vladu, E. D. Glowacki, N. S. Sariciftci, S. Bauer, *Green Materials for Electronics*, John Wiley & Sons, New York **2017**.
- [28] L. Q. Khor, K. Y. Cheong, *J. Mater. Sci.: Mater. Electron.* **2013**, *24*, 2646.
- [29] J. Heinze, B. A. Frontana-Urbe, S. Ludwigs, *Chem. Rev.* **2010**, *110*, 4724.
- [30] C. M. Proctor, J. Rivnay, G. G. Malliaras, *J. Polym. Sci., Part B: Polym. Phys.* **2016**, *54*, 1433.
- [31] M. Berggren, G. G. Malliaras, *Science* **2019**, *364*, 233.
- [32] W. Yang, J. Xu, Y. Yang, Y. Chen, Y. Zhao, S. Li, Y. Jiang, *J. Mater. Sci.: Mater. Electron.* **2015**, *26*, 1668.
- [33] M. F. Ashby, D. Cebon, *J. Phys. IV* **1993**, *3*, C7.
- [34] J. Rivnay, S. Inal, A. Salleo, R. M. Owens, M. Berggren, G. G. Malliaras, *Nat. Rev. Mater.* **2018**, *3*, 17086.
- [35] J. Rivnay, P. Leleux, M. Ferro, M. Sessolo, A. Williamson, D. A. Koutsouras, D. Khodagholy, M. Ramuz, X. Strakosas, R. M. Owens, C. Benar, J. Badier, C. Bernard, G. G. Malliaras, *Sci. Adv.* **2015**, *1*, e1400251.
- [36] H. H. Choi, K. Cho, C. D. Frisbie, H. Siringhaus, V. Podzorov, *Nat. Mater.* **2018**, *17*, 2.
- [37] V. Podzorov, *MRS Bull.* **2013**, *38*, 15.
- [38] Q. Wei, M. Mukaida, Y. Naitoh, T. Ishida, *Adv. Mater.* **2013**, *25*, 2831.
- [39] A. Sajjad, S. Subhani Sajjad, *J. Dent. Surg.* **2014**, *2014*, 210463.
- [40] N. K. Logothetis, C. Kayser, A. Oeltermann, *Neuron* **2007**, *55*, 809.
- [41] T. N. Shatskikh, M. Raghavendra, Q. Zhao, Z. Cui, G. L. Holmes, *Epilepsy Behav.* **2006**, *9*, 549.
- [42] J. N. Gelinas, D. Khodagholy, T. Thesen, O. Devinsky, G. Buzsáki, *Nat. Med.* **2016**, *22*, 641.
- [43] H. Yuk, B. Lu, X. Zhao, *Chem. Soc. Rev.* **2019**, *48*, 1642.